

Spectroscopy of Coherent Dark Resonances in Multilevel Atoms for the Example of Samarium Vapor

Yu. V. Vladimirova^a, B. A. Grishanin^{a,*}, V. N. Zadkov^{a,**},
N. N. Kolachevskii^b, A. V. Akimov^b, N. A. Kisilev^b, and S. I. Kanorskiĭ^b

^aDepartment of Physics and the International Laser Center, Moscow State University, Moscow, 119899 Russia

^bLebedev Physical Institute, Russian Academy of Sciences, Moscow, 117924 Russia

*e-mail: grishan@comsim1.phys.msu.su

**e-mail: zadkov@comsim1.phys.msu.su

Received August 30, 2002

Abstract—A universal theory for calculating coherent population trapping resonances in multilevel atoms is suggested. The theory allows arbitrary schemes of multilevel atoms and their excitations to be calculated taking into account the influence of relaxation effects in atoms, applied magnetic field, and the Doppler effect. The experimental data obtained by high-precision diode spectroscopy of coherent dark resonances in samarium vapor are systematically analyzed using the suggested theory. In the absence of a magnetic field, the model of samarium is based on consideration of a degenerate Λ system of the $4f^6 6s^2(^7F_0) \longleftrightarrow 4f^6(^7F)6s6p(^3P^0)^9F_1^0 \longleftrightarrow 4f^6 6s^2(^7F_1)$ active transitions. If the fourth $4f^6 6s^2(^7F_2)$ level is taken into account, this Λ system becomes open. Numerical simulation of coherent population trapping resonances shows that the open character of the system decreases the contrast of resonance curves in absorption spectra without changing resonance widths. The system under applied external longitudinal and transverse magnetic fields is correctly described by 7- and 12-level models of atomic transitions, respectively. © 2003 MAIK “Nauka/Interperiodica”.

1. INTRODUCTION

The interaction of an electromagnetic field with an atom is one of the most fundamental problems of quantum optics. Multilevel atoms are known to exhibit a broader spectrum of effects under these conditions than two-level atoms because of field-induced coherence between atomic states and quantum interference. Three-level systems in the Λ , Ξ , and V configurations play an important role in studying these effects, being intermediate in complexity between two-level and multilevel atoms. Quite a number of new effects are observed in three-level atoms, of which coherent population trapping is one of the most intriguing phenomena. This phenomenon has been extensively studied both theoretically and experimentally (see review [1] and the references therein). The coherent population trapping effect most strikingly manifests itself in three-level systems with two closely spaced long-lived levels and the third level distant from them (Λ or V systems), which are excited by two continuous laser fields in such a way that the distant level is optically “coupled” with two others. Tuning the exciting fields in resonance with dipole transitions results in system population trapping in the coherent superposition of two closely spaced levels. This effect manifests itself in Raman absorption spectra as a very narrow dip against the absorption line background and in resonance fluorescence spectra as

the absence of emission, whence the term “dark (or coherent population trapping) resonance.”

The coherent population trapping phenomenon is currently extensively used in various applications, such as magnetometry, metrology, etc. [2–6]. Since the first observation of a coherent population trapping resonance in sodium vapor [2], the majority of experimental studies of coherent population trapping resonances have been performed with alkali metal atoms [1, 7], whose hyperfine ground state components with characteristic splittings of several GHz were used as the lower Λ system levels. The long lifetimes of the coherent superposition of the lower alkali metal atom states allow high-contrast and high- Q coherent population trapping resonances to be recorded thanks to the availability of stable high-precision laser systems tunable in resonance transition regions and comparatively simple phase locking of exciting light fields. For instance, resonances about 10 kHz wide were recorded for pure cesium vapor [7]. A further decrease in the width of resonances can be achieved by introducing an inert buffer gas (Ne, He, or Ar) into the cell for measurements at pressures of several kPa. The residence time of atoms in light beams then increases without disturbing coherence of the superposition state of the lower levels, which are weakly dephased by collisions with buffer gas atoms. In particular, the narrowest resonance about

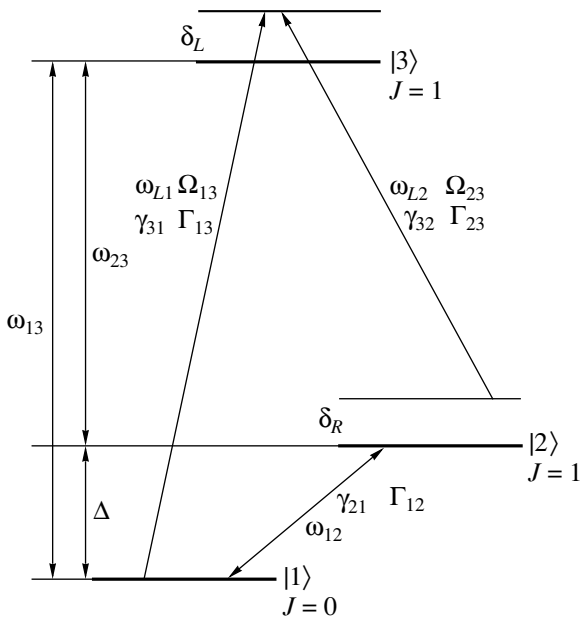


Fig. 1. Scheme of a three-level atom in the Λ configuration excited by two laser fields at frequencies ω_{L1} and ω_{L2} . Ω_{13} and Ω_{23} are the Rabi frequencies corresponding to pumping fields; δ_L is the resonance detuning at the $|1\rangle \longleftrightarrow |3\rangle$ transition; δ_R is the Raman detuning; γ_{31} and γ_{32} are the rates of radiative decay of excited states to the $|1\rangle$ and $|2\rangle$ levels, respectively; γ_{21} and w_{12} are the rates of decay and thermal pumping of level $|1\rangle$ through $|2\rangle$; and Γ_{13} , Γ_{23} , and Γ_{12} are the rates of dephasing of transitions $|1\rangle \longleftrightarrow |3\rangle$, $|2\rangle \longleftrightarrow |3\rangle$, and $|1\rangle \longleftrightarrow |2\rangle$, respectively.

50 Hz wide was obtained for cesium–neon combinations [7].

Coherent population trapping in rare-earth metal atoms has certain special features, because the characteristic distance between fine structure components used as the lower Λ system levels is substantially larger than the hyperfine splittings of alkali metal ground states and amounts to 10–100 THz. The characteristic spontaneous decay time of these levels is determined by magnetic dipole transitions and equals several seconds, which does not prevent the observation of supernarrow resonances. These levels are also weakly sensitive to atomic collisions, because they are well shielded by the outer closed shell. For this reason, rare-earth metal atoms also offer promise for use in metrological applications, for instance, for creating a secondary frequency standard (e.g., see [8]). The samarium atom is one of the most promising objects for metrological applications. Its scheme of levels is much simpler than that of cesium, especially in applied magnetic fields. Precisely for this reason, we selected it as a “touchstone” for testing the general theory of coherent population trapping in multilevel atoms developed by us.

Theoretically, the coherent population trapping phenomenon was studied in detail for the three-level model [1], which allows calculations to be performed

analytically. The model, however, becomes much more complex for multilevel systems, and its analytic study turns impossible in the majority of cases. In this work, we suggest a general theoretical model for numerically analyzing the coherent population trapping spectra of atoms with an arbitrary number of levels and compare the results obtained for this model with the experimental data on samarium [9].

In Section 2, we describe the coherent population trapping effect in terms of the simplest three-level Λ system model. Section 3 contains a description of a general mathematical technique for calculating stationary states of active atoms and the corresponding level populations, absorption coefficients, and the dispersion of applied fields from the point of view of the spectroscopy of dark resonances. A method for taking into account the Doppler effect in calculating medium absorption is considered in Section 4. An experimental study of coherent population trapping in samarium vapor is described in Section 5. For samarium atoms, completely taking into account the Zeeman structure of lines involved in the formation of coherent population trapping resonances requires the use of a 12-level model. However, even a substantially simpler 4-level model gives close qualitative agreement with experiment. Section 6 contains a general description of this model and parameters necessary for performing calculations and comparing them with experimental results. The results obtained in calculating absorption in the absence of magnetic fields and under longitudinal and transverse applied fields are given in Section 7, where these results are compared with experimental data. The most important conclusions are formulated in Section 8. The special features of coherent population trapping resonances against the background of a line broadened by the Doppler effect in longitudinal and transverse magnetic fields are considered in the Appendix.

2. COHERENT POPULATION TRAPPING IN A Λ SYSTEM

In the simplest three-level system of atomic transitions in the Λ configuration, two lower long-lived levels $|1\rangle$ and $|2\rangle$ with frequency splitting Δ are coupled with the upper excited energy level $|3\rangle$ by two light fields (Fig. 1). If the $|1\rangle \longleftrightarrow |2\rangle$ transition is forbidden in the dipole approximation and two fields $E_1 \exp(-i\omega_{L1}t - i\varphi_1)$ and $E_2 \exp(-i\omega_{L2}t - i\varphi_2)$ are in resonance with the corresponding $|1\rangle \longleftrightarrow |3\rangle$ and $|2\rangle \longleftrightarrow |3\rangle$ transitions, a narrow coherent population trapping resonance is formed as a result of quantum interference. It manifests itself in absorption spectra by the appearance of a sharp maximum when one of the acting fields, for instance, ω_{L1} , is scanned and the Raman detuning $\delta_R = \omega_{L1} - \omega_{L2} - \Delta$ passes zero, which corresponds to the exact resonance.

To describe the nature of this physical process more visually, different basis sets are used to consider the

atomic system. In particular, the $|1\rangle$ and $|2\rangle$ ground states can conveniently be replaced by their symmetrical and antisymmetric combinations $|\pm\rangle$,

$$|+\rangle = \frac{\Omega_{R1}^*|1\rangle + \Omega_{R2}^*|2\rangle}{\Omega_{\text{eff}}}, \quad |-\rangle = \frac{\Omega_{R2}|1\rangle - \Omega_{R1}|2\rangle}{\Omega_{\text{eff}}},$$

where $\Omega_{Rk} = -d_{3k}E_k/\hbar$ ($k = 1, 2$) are the Rabi frequencies determined from the corresponding dipole moments $d_{3k} = -e\langle 3|r|k\rangle$,

$$\Omega_{\text{eff}} = \sqrt{|\Omega_{R1}|^2 + |\Omega_{R2}|^2}$$

is the effective Rabi frequency, and the phases of states $|1\rangle$ and $|2\rangle$ coincide with those of laser fields.

The matrix element of the electric dipole operator between the ground and excited states vanishes for the $|-\rangle$ state at zero Raman detuning,

$$\langle 3|V_{\text{dip}}|-\rangle \propto (1 - e^{i\delta_R t}) \xrightarrow{\delta_R \rightarrow 0} 0.$$

By far the larger part of atomic population is concentrated in this state named dark because of radiative decay. As a result, fluorescence is almost fully suppressed. This process of optical pumping into the coherent dark state is known as coherent population trapping. The coherent nature of population trapping manifests itself by a dependence of the dark state on laser field phases. It follows that acting field phase fluctuations can decrease or even destroy coherent population trapping, and it is necessary to stabilize the relative phase of laser fields. Other decoherence processes and Doppler broadening can also contribute to the destruction of coherent population trapping.

The experimentally observed line width is determined by the stability of detuning δ_R and phase difference $\Delta\phi$ and also by Doppler broadening, time-of-flight broadening, Stark broadening (broadening caused by light and external fields), broadening in nonuniform magnetic fields, and impact broadening. The $\Delta\phi$ phase difference can very accurately be stabilized in experiments with alkali metal atoms, for instance, by modulating lasers at a frequency corresponding to Δ . When two independent diode lasers are used in the free generation mode, we can expect that coherent population trapping resonances several MHz wide will be observable.

3. A MATHEMATICAL TECHNIQUE FOR CALCULATING COHERENT POPULATION TRAPPING IN MULTILEVEL SYSTEMS

A description of the dynamics of quantum systems in which relaxation processes occur requires modifying dynamic equations in comparison with their usual form given in traditional textbooks on quantum mechanics and only applicable to closed systems without relaxation. While the dynamics of closed systems is determined by an energy operator acting on wave functions,

the dynamics of systems with relaxation can only be described by transformations of density matrix operators or of dynamic variables, that is, by superoperator transformations. The simplest transformations of this type also arise in systems without relaxation if these systems are described in terms of density matrices, in particular, by the Liouville quantum equation

$$\frac{\partial \hat{\rho}}{\partial t} = \mathcal{L}_0 \hat{\rho} = -\frac{i}{\hbar} [\hat{H}, \hat{\rho}].$$

The role of a superoperator transformation is here played by the Liouvillian \mathcal{L}_0 . To the $-i/\hbar$ imaginary factor, the Liouvillian is described by the commutator with Hamiltonian \hat{H} applied to the density matrix $\hat{\rho}$.

In order to introduce the corresponding superoperators irrespective of the operators to be transformed, it suffices to introduce the substitution symbol \odot for specifying the position into which the operator in question should be substituted. In the Schrödinger representation, this is the density matrix. Further, we can use the rules for handling symbolic expressions that follow from the general definitions of the algebra of linear operators [10], which are quite obvious. For instance,

$$\begin{aligned} [\hat{A}_2, [\hat{A}_1, \odot]] &= \hat{A}_2(\hat{A}_1 \odot - \odot \hat{A}_1) - (\hat{A}_1 \odot - \odot \hat{A}_1) \hat{A}_2 \\ &= \hat{A}_2 \hat{A}_1 \odot - \hat{A}_1 \odot \hat{A}_2 - \hat{A}_2 \odot \hat{A}_1 + \odot \hat{A}_1 \hat{A}_2. \end{aligned}$$

In the symbolic representation, the Liouvillian of a closed system has the form

$$\mathcal{L}_0 = -\frac{i}{\hbar} [\hat{H}, \odot]. \quad (1)$$

Like all linear operators, superoperators can be written in the form of the corresponding matrices after the introduction of a linear basis in the linear space of quantum operators. The use of this technique for symbolically representing superoperators is effective in calculating systems of arbitrary dimensions, especially in calculating multilevel systems. In particular, because of large problem dimensions, even merely writing down the matrices that describe the evolution superoperators becomes a technically complex task. However, if the symbolic representation of superoperators is used, these matrices can first be written in the symbolic form thanks to its physical transparency, and matrix elements can then be calculated either analytically or numerically (for large-dimensionality matrices) on a computer. Technical difficulties of reproducing them are then fully transferred to automatic computer calculations, and the results of such calculations can easily be used in numerical calculations of applied problems under consideration with programs written in the most suitable programming language. We used a combination of the MATHEMATICA computer algebra package (for analytically setting superoperators) and the Fortran language (for subsequent numerical calculations of spectra with the use of the calculated dynamic superoperator matrices).

3.1. Calculations of the Liouvillian of an N -Level Atom in the Symbolic Representation

As for the two-level system, the Liouvillian of an N -level atom in the rotating field approximation can be written as the sum of contributions

$$\mathcal{L}_t = \mathcal{L}_r + \mathcal{L}_e + \mathcal{L}_\delta + \mathcal{L}_i, \quad (2)$$

where \mathcal{L}_r is the radiative damping superoperator, \mathcal{L}_e is the elastic dephasing superoperator, \mathcal{L}_i is the superoperator of the interaction with the laser field, and \mathcal{L}_δ is the laser detuning superoperator, which augments the selected unperturbed evolution operator to the superoperator of free atomic dynamics in zero laser field. It includes the corresponding detunings of all acting laser fields and takes into account that free precession at the frequencies of these fields is included into the unperturbed dynamics superoperator.

Radiative damping is described by the Liouvillian that combines the population transfer superoperator given by the $\hat{P}_{lk} \odot \hat{P}_{kl}$ projector and the polarization damping superoperator given by the $[\hat{P}_{kk}, \odot]_+$ anticommutator,

$$\mathcal{L}_r = \sum_{kl} \gamma_{kl} \left(\hat{P}_{lk} \odot \hat{P}_{kl} - \frac{1}{2} [\hat{P}_{kk}, \odot]_+ \right), \quad (3)$$

where the two-dimensional array γ_{kl} describes the rates of spontaneous decay (for $k > l$) and pumping (for $k < l$).

Elastic dephasing is introduced by the \mathcal{L}_e superoperator written in terms of the squares of commutators and determined by the particular model of dephasing. In order to specify it, consider two types of dephasing. First, we can only take into account internal dephasing in the system of two electronic states k and $l > k$. In conformity with the microscopic nature of elastic dephasing caused by weak collisions [11, 12] (random transition frequency fluctuations), this dephasing is described by the corresponding random frequency shift superoperator $-(i/2)\xi(t)[(\hat{P}_{kk} - \hat{P}_{ll}), \odot]$, where $\xi(t)$ is the fluctuation transition frequency shift. The resulting relaxation superoperator averaged over random phase fluctuations has the form

$$\mathcal{L} = -\frac{\Gamma_{in}^{kl}}{4} [\hat{n}_{kl}, \odot]^2,$$

where $\hat{n}_{kl} = \hat{P}_{ll} - \hat{P}_{kk}$ is the population inversion operator for the kl subsystem and Γ_{in}^{kl} is the corresponding dephasing rate. This type of pure dephasing is not only related to the dephasing of the kl transition itself but also contributes to the dephasing of all the transitions adjacent to it. It is nevertheless convenient to consider

the dephasing only of the kl transition with the use of the representation

$$[\hat{n}_{kl}, \odot]^2 = 2(\hat{P}_{kk} \odot \hat{P}_{ll} + \hat{P}_{ll} \odot \hat{P}_{kk}) + [\hat{I}_{kl}, \odot]^2,$$

where $\hat{I}_{kl} = \hat{P}_{ll} + \hat{P}_{kk}$ is the operator of the total population of the kl subsystem. The first term,

$$\mathcal{L}_{in}^{kl} = -\Gamma_{in}^{kl}(\hat{P}_{kk} \odot \hat{P}_{ll} + \hat{P}_{ll} \odot \hat{P}_{kk}), \quad (4)$$

describes purely internal dephasing and does not influence adjacent transitions. Using all Γ_{in}^{kl} independent parameters, we can write the dephasing of all transitions by (4) alone. For simplicity of describing the physical nature of dephasing, it is, however, convenient to introduce another contribution. This is equal dephasings of arbitrary other levels through the k th and l th levels in the absence of action on the kl transition itself, that is, “external dephasing,”

$$\mathcal{L}_{ex}^{kl} = -\Gamma_{ex}^{kl} [\hat{I}_{kl}, \odot]^2, \quad (5)$$

where Γ_{ex}^{kl} is the corresponding dephasing rate. Accordingly, the complete elastic dephasing superoperator is given by the sum

$$\mathcal{L}_e = \sum_{k < l} (\mathcal{L}_{in}^{kl} + \mathcal{L}_{ex}^{kl}). \quad (6)$$

The laser detuning superoperator depends on the type of resonance under consideration and can usually be written in the form of an antisymmetric superoperator given by the commutator with population operators,

$$\mathcal{L}_\delta = i \sum_k \delta_k (\hat{P}_{kk} \odot - \odot \hat{P}_{kk}), \quad (7)$$

where δ_k is the array of frequency detunings.

The interaction with the laser field can be described by the antisymmetric commutator with the polarization operators

$$\mathcal{L}_i = -\frac{i}{2} \sum_{k < l} \Omega_{kl} [(\hat{P}_{kl} + \hat{P}_{lk}), \odot], \quad (8)$$

where Ω_{kl} is the two-dimensional array of the Rabi frequencies of the kl transitions.

After the introduction of the symbolic representation of the complete evolution operator [Eq. (2)] and its components (3) and (6)–(8), we can calculate the $N^2 \times N^2$ matrix representations of the \mathcal{L}_t , \mathcal{L}_r , \mathcal{L}_e , \mathcal{L}_δ , and \mathcal{L}_i values by the formula

$$L_{mn} = (\hat{e}_m, \mathcal{L} \hat{e}_n).$$

Here, $\{\hat{e}_k\}$ is the orthonormalized basis and parentheses denote the scalar multiplication of two operators of

the form $\text{Tr}(\hat{A}^+ \hat{B})$, which is antilinear in the first and linear in the second multiplier.

The $\{\hat{e}_k\}$ basis can conveniently be selected as Hermitian and expressed via the \hat{P}_{kl} transition operators represented by $N \times N$ matrices, each with a single non-zero kl element $P_{kl}(k, l) = 1$. It is also convenient to assume that the levels are numbered in order of increasing energy, $E_1 \leq E_2 \leq \dots \leq E_N$. The corresponding basis is then constructed as follows:

$$\hat{e}_{j(k,l)} = \begin{cases} \hat{P}_{kk}, & k = l, \\ \frac{\hat{P}_{kl} + \hat{P}_{lk}}{\sqrt{2}}, & k < l, \\ -i \frac{\hat{P}_{kl} - \hat{P}_{lk}}{\sqrt{2}}, & k > l, \end{cases} \quad (9)$$

where $j(k, l)$ is the numbering index, that is, a one-to-one mapping of the two-dimensional set of numbers kl ($k, l = 1, N$) onto the one-dimensional set $j = 1, N^2$. This index can, in particular, be specified in the following way universal for any N :

$$j = \begin{cases} k, & k = l, \\ (2k-1)N - (k+1)^2 + k + 2l, & k < l, \\ (2l-1)N - (l+1)^2 + l + 2k + 1, & k > l. \end{cases}$$

For $N = 2, 3$, and 4 , this corresponds to the following $j_N = (j_N(k, l))$ matrices:

$$j_2 = \begin{pmatrix} 1 & 3 \\ 4 & 2 \end{pmatrix}, \quad j_3 = \begin{pmatrix} 1 & 4 & 6 \\ 5 & 2 & 8 \\ 7 & 9 & 3 \end{pmatrix},$$

$$j_4 = \begin{pmatrix} 1 & 5 & 7 & 9 \\ 6 & 2 & 11 & 13 \\ 8 & 12 & 3 & 15 \\ 10 & 14 & 16 & 4 \end{pmatrix}.$$

Basis (9) is Hermitian and orthonormalized with respect to the (\hat{A}, \hat{B}) scalar product described above, and $(\hat{e}_m, \hat{e}_n) = \delta_{mn}$ for all $m, n = 1, N^2$.

3.2. Calculations of Coherent Population Trapping in an N -Level Atom

The technique described above can effectively be used in analytic calculations for solving the stationary state problem and the complete spectral problem for the \mathcal{L}_t evolution superoperator [13, 14].

The most important properties of coherent population trapping are determined by the absorption of applied field. For the Λ resonance, absorption is described by the equation

$$W_L = \hbar \text{Im}(\omega_L g \langle \hat{\sigma}_{13}^+ \rangle + \omega'_L g' \langle \hat{\sigma}_{23}^+ \rangle) \approx \hbar(\omega_L \gamma + \omega'_L \gamma') n_3. \quad (10)$$

Here, $\langle \hat{\sigma}_{13}^+ \rangle$ and $\langle \hat{\sigma}_{23}^+ \rangle$ are averaged positive-frequency operators of the complex amplitudes of the 1–3 and 2–3 transitions, respectively; ω_L and ω'_L are the frequencies of biharmonic pumping fields; g and g' are the corresponding Rabi frequencies; and γ and γ' are the corresponding radiative damping rates. The determination of the $\langle \hat{\sigma}_{13}^+ \rangle$, $\langle \hat{\sigma}_{23}^+ \rangle$, or n_3 stationary mean values requires calculating the corresponding vector representation $\langle 0|$ of the $\hat{\rho}_{st}$ stationary density matrix by solving the $\langle 0| L_t = 0$ equation.

In the basis under consideration with $\hat{e}_1 = \hat{P}_{11}$, $\hat{e}_2 = \hat{P}_{22}$, and $\hat{e}_3 = \hat{P}_{33}$, the first three vector $\langle 0|$ elements describe populations and should be normalized accordingly. The $\langle 0|$ bra vector of the stationary density matrix should therefore be used in the normalized form

$$\langle 0| \rightarrow \frac{\langle 0|}{\langle 0|_1 + \langle 0|_2 + \langle 0|_3},$$

which automatically gives correct signs of the values to be calculated. The mean populations then coincide with the corresponding components, $\langle \hat{n}_k \rangle = \langle 0|_k$, $k = 1, 3$, and the complex transition amplitudes are expressed through the components with $k > 3$,

$$\langle \hat{\sigma}_{13}^+ \rangle = \frac{\langle 0|_6 + i\langle 0|_7}{\sqrt{2}}, \quad \langle \hat{\sigma}_{23}^+ \rangle = \frac{\langle 0|_8 + i\langle 0|_9}{\sqrt{2}},$$

$$\langle \hat{\sigma}_{12}^+ \rangle = \frac{\langle 0|_4 + i\langle 0|_5}{\sqrt{2}}.$$

These equations allow absorption to be written in an analytic form convenient for both numerical calculations and a qualitative analysis.

We wrote a universal Fortran program for calculating level populations, absorption coefficients, and dispersion in an arbitrary N -level system. The program can be used at large $N > 10$ values. Its important feature is the use of a minimum necessary number of input parameters, which is substantially smaller than the $N^2 \times N^2$ number of Liouvillian matrix elements in the Liouvillian generalization under consideration [Eq. (1)], because it is not necessary to write down all L_t dynamic matrix elements by hand. According to (2)–(8), this matrix in reality contains a huge number of zero contributions.

4. TAKING INTO ACCOUNT THE DOPPLER EFFECT

The technique of calculations described in Section 3 can be used to obtain the dependences of the laser radiation absorption coefficient for an atom at rest on the first field δ_L and Raman δ_R detunings. In experiments, moving atoms interact with fields. For this reason, the Doppler effect influences the absorption coefficient of the medium. In the absence of simplifications, this requires performing calculations for a continuum of detunings simultaneously. In this work, the Doppler effect was taken into account by the following simplified method, which qualitatively corresponds to the approach taken in [15], but without approximately replacing the Maxwell velocity distribution by the Lorentz distribution.

The frequency of the laser field that interacts with an atom that moves in an arbitrary direction is given by the formula $\omega_{1,2} = \omega_{Lj} + \delta_{Lj}$, which takes into account the first-order correction for the Doppler effect. Here, $\delta_{Lj} = \omega_{Lj} v_n / c$, $j = 1, 2$, are the detunings of the biharmonic laser field components and v_n is the projection of the velocity of the moving atom onto the vector \mathbf{n} of laser beam propagation.

The number of gas particles that move at velocity v_k at temperature T is determined by the Maxwell velocity distribution [11]

$$\frac{dN}{d\delta_L} = \frac{N}{\sqrt{\pi}} \exp\left[-\left(\frac{\delta_L}{\Delta\omega_D}\right)^2\right] \frac{d\delta_L}{\Delta\omega_D}, \quad \Delta\omega_D = \frac{\omega_{L1} v_0}{c},$$

where

$$\delta_L = \omega - \omega_{L1}, \quad v_0 = \sqrt{\frac{2kT}{m}}.$$

The $\delta_R = \omega_{L2} - \omega_{L1} - \Delta$ Raman detuning for laser beams propagating in one direction is then considered approximately constant for particles moving at differ-

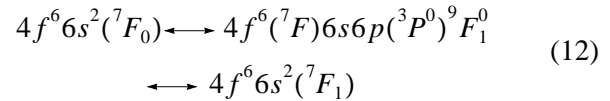
ent velocities. The dependence of the absorption coefficient for field ω_{L1} on the Raman detuning when field ω_{L2} is scanned therefore has the form

$$K_D(\delta_R) = \int K(\delta_L, \delta_R) \frac{dN}{d\delta_L} d\delta_L, \quad (11)$$

where $K(\delta_L, \delta_R)$ is the absorption coefficient of the atom at rest.

5. EXPERIMENTAL OBSERVATION OF COHERENT POPULATION TRAPPING RESONANCES IN SAMARIUM VAPOR

As mentioned in Section 1, samarium is a promising candidate for studying the feasibility of using coherent population trapping resonances in rare-earth metal vapors for metrological application purposes by high-resolution nonlinear spectroscopy methods. A diagram of the energy levels of the samarium atom is shown in Fig. 2. We experimentally studied samarium vapor absorption in the region of the



transition lines, which formed a Λ system.

The experimental unit is schematically drawn in Fig. 3. The radiation sources were two semiconductor lasers (1, 2) with external cavity resonators tuned to resonance wavelengths 672 and 686 nm. The lasers were assembled according to the Littrow scheme with a collimating aspherical objective and a holographic grating of 1800 lines/mm. The free detuning range of lasers was around 5 GHz. The lasers, with radiation wavelengths 672 and 686 nm, radiated 2.5 and 12 mW, respectively, in the single-frequency mode.

The spectra of the transitions in samarium that we were interested in were studied in detail in [16] by sub-

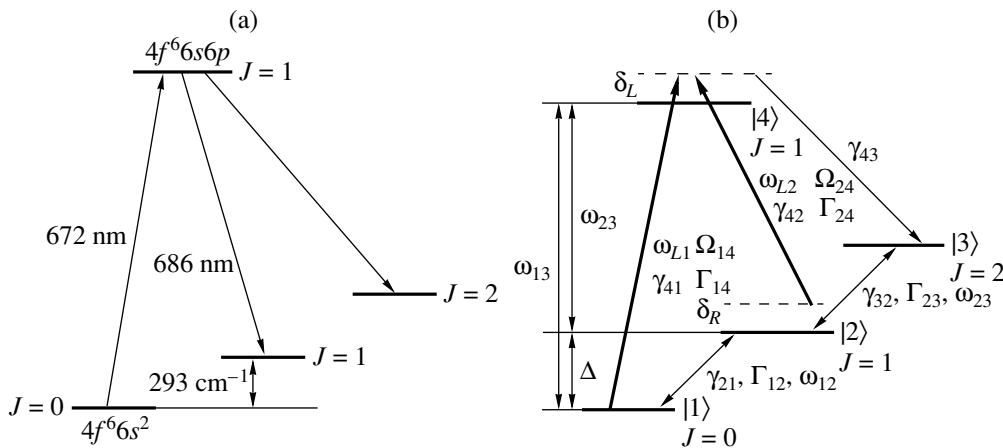


Fig. 2. (a) Diagram of energy levels of the samarium atom and (b) parameters used in calculations. The notation is the same as in Fig. 1 (for the corresponding level numbers).

Doppler absorption saturation spectroscopy. In [16], the relative isotopic shifts and hyperfine splittings of the levels were determined accurate to 1–2 MHz. The ^{154}Sm isotope (abundance 22.75%) had lines shifted with respect to the spectral lines of the other isotopes [^{144}Sm (3.07%), ^{147}Sm (14.99%), ^{148}Sm (11.24%), ^{149}Sm (13.82%), ^{150}Sm (7.38%), and ^{152}Sm (26.75%)] by 1 GHz to the red, which allowed reliable frequency locking to the transitions in this isotope to be performed. The presence of the other isotopes, however, slightly changed the wings of the working transition line.

Samarium vapor was generated in stainless steel cell 7, which was 50 cm long and had glass windows at the ends. The cell was connected to a vacuum line and a system for buffer gas puffing. The cell was heated in its central part (15 cm long) with coaxial direct-current heater 8 (~500 W). The remanent magnetic field in the cell was of fractions of an oersted unit. The cell was placed within two pairs of Helmholtz rings 9 30 cm in diameter, which could be used to create longitudinal and transverse magnetic fields up to 40 Oe in the central part of the cell. To obtain noticeable absorption, the cell was heated to about 1000 K [9]. Vapor concentration at this temperature was about 10^{11} – 10^{12} cm^{-3} .

The 672 nm laser was tuned to the center of the $4f^66s^2(^7F_0) \longleftrightarrow 4f^66s6p(^9F_1^0)$ transition in ^{154}Sm and locked to the transmission peak of stabilized one-meter confocal interferometer 12 with a high long-term stability (about 5 MHz/h). The width of the laser generation spectrum was less than 0.5 MHz. The 686 nm laser was slowly retuned in the region of the $4f^66s^2(^7F_1) \longleftrightarrow$

$4f^66s6p(^9F_1^0)$ transition in such a way that its frequency passed the $\delta_R = 0$ point. Laser generation frequency variations were controlled by 0.5-m confocal interferometer 13 with a Q -factor of about 20 and a free dispersion region of 149.8 ± 0.1 MHz. The mode composition of laser radiation was controlled using spectrum analyzer 14 with a Q -factor of 50 and a free dispersion region of 8 GHz. All interferometers were optically isolated from lasers to prevent the arising of feedback. Linearly polarized laser radiation converged into one beam (accurate to 10^{-3} rad) on polarization cube 6 and was launched into the cell with samarium vapor. The polarization planes of the beams were mutually orthogonal. At the entrance to the cell, radiation power density was 0.1 mW/mm² for the 672 nm laser and 0.2 mW/mm² for the 686 nm laser. After exit from the cell, the beams were divided using holographic diffraction grating 15 (2400 lines/mm) and directed to a system for recording (components 16, 20, and 21).

As coherent population trapping is related to atomic system interactions with a dichromatic light field, we only recorded changes in the adsorption of laser radiation at 672 nm caused by the presence of the second light field. For this purpose, the beam from the 686 nm

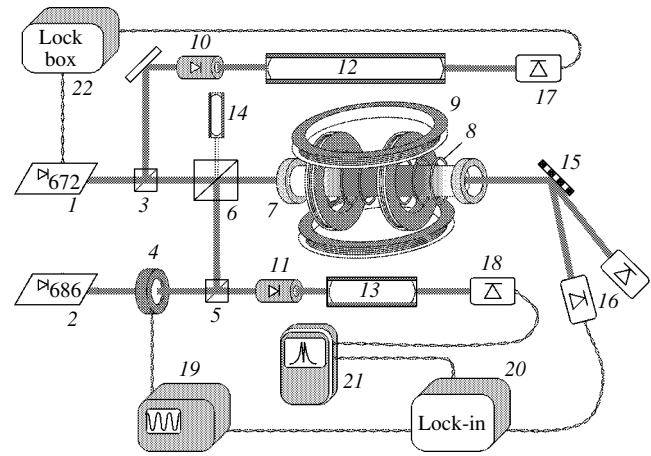


Fig. 3. Experimental unit for measuring dark resonance spectra in samarium vapor; 1 and 2 are semiconducting lasers with 672 and 686 nm wavelengths, respectively; 3 and 5 are light-splitting cubes; 4 is a modulator (600 Hz frequency); 6 is a polarizing cube; 7 is a cell with samarium vapor; 8 is a coaxial heater; rings 9 are Helmholtz rings; 10 and 11 are optical insulators; 12 is a confocal interferometer with the region of free dispersion of 74.35 ± 0.01 MHz; 13 is a confocal interferometer with the region of free dispersion of 149.8 ± 0.01 MHz; 14 is a spectroanalyzer; 15 is a 2400 lines/mm diffraction grating; 16–18 are photodiodes; 19 is a generator; 20 is a synchronous detector; 21 is an oscilloscope with memory; and 22 is the electronic block for locking the 672 nm laser frequency to the transmission peak of interferometer 12.

laser was modulated by liquid crystalline modulator 4 at a frequency of $f_m = 600$ Hz before it entered the cell, and the signal with the same modulation frequency was recorded in the channel of the 672 nm laser. The presence of broad excess absorption wings was caused by collisions with buffer gas atoms [17]. The spectra of induced absorption were recorded at both zero magnetic field and under applied longitudinal and transverse magnetic fields. In experiments with transverse applied fields, their direction was aligned with the direction of 672 nm laser polarization.

6. COHERENT POPULATION TRAPPING IN THE FOUR-LEVEL MODEL

In the experiment under consideration, apart from the active samarium vapor levels that formed the Λ system, the formation of coherent population trapping resonances involved the $4f^66s^2$ ($J = 2$) level. Although this level did not directly participate in the excitation of the upper level, it absorbed part of the population as a consequence of radiative decay (Fig. 2a). In addition, the $J = 2$ level was populated by incoherent pumping from the lower levels that formed the Λ system. It follows that the $J = 2$ level played the role of a reservoir for coherent population trapping in the Λ system under consideration and its presence made the Λ system an open system. In the absence of magnetic field, this four-

Table 1. Wavelengths and oscillator strengths of active transitions

Transition	Wavelength λ , nm	Oscillator strength gf
$6s^2 (J=0) \rightarrow 6s6p (J=1)$	672.5875	8.5×10^{-3}
$6s^2 (J=1) \rightarrow 6s6p (J=1)$	686.0927	9.5×10^{-3}

level model takes into account the main mechanisms that determine coherent population trapping effects.

The characteristics of the samarium atom and the parameters of experiments necessary for a comparison with experimental data are summarized in Tables 1, 2, and 3. Table 1 contains the oscillator strengths of the transitions of interest, and Table 2, the energies and g -factors of the lower metastable levels with $J = 0, 1$, and 2 and the upper level of the Λ system. The relative populations of the metastable levels at $T = 600^\circ\text{C}$ are also given (see [16]).

Dipole moment d , Rabi frequencies Ω , and decay rates γ are calculated by the equations

$$|d_{JJ'}|^2 = \frac{3\hbar e^2 (2J+1) |f_{JJ'}|}{2m \omega_{JJ'}},$$

$$\Omega_{JJ'} = \frac{d_{JJ'} E}{\hbar}, \quad \gamma_{JJ'} = \frac{4d_{JJ'}^2 \omega^3}{3\hbar c^3},$$

where m and e are the mass and the charge of the electron, respectively; c is the velocity of light; $\omega_{JJ'}$ is the transition frequency; and $|f_{JJ'}|$ is the oscillator strength of the $J \rightarrow J'$ transition. The electric fields are calculated by the formula $E = \sqrt{2W/c\epsilon_0}$; they take on the values $E_{L1} \approx 270$ V/m and $E_{L2} \approx 390$ V/m at laser radiation power densities at the entrance to the cell of $W_{L1} = 0.1$ mW/mm² and $W_{L2} = 0.2$ mW/mm², respectively [9]. The calculation results are summarized in Table 3.

The longitudinal and transverse magnetic field intensities were 15 and 29 Oe, respectively. The Zeeman splittings in the longitudinal magnetic field calculated as $\Delta = egH/2mc$ were $\Delta' = 1.98 \times 10^8$ s⁻¹ for the $6s6p$ level and $\Delta'' = 4.09 \times 10^8$ s⁻¹ for the $6s^2$ level. The

transverse magnetic field splittings were $\Delta' = 2.50 \times 10^8$ s⁻¹ for the $6s6p$ level and $\Delta'' = 5.17 \times 10^8$ s⁻¹ for the $6s^2$ level.

7. THE RESULTS OF SIMULATING THE COHERENT POPULATION TRAPPING SPECTRA IN SAMARIUM VAPOR

Calculations based on the technique described in Section 3 gave the absorption coefficients of a samarium atom at rest for the three- and four-level models (Figs. 4a and 4b, respectively). An analysis of the dependences plotted in these figures shows that the introduction of the fourth $J = 2$ level into the three-level model has virtually no effect on the width of the resonance, whereas the complete absorption value for the four-level system is much smaller than for the three-level one. The reason for this is population trapping at the $J = 2$ level through the corresponding radiative decay channel.

7.1. The Modification of the Spectra in a Magnetic Field

Applying magnetic field transforms the three-level system of the samarium atom considered above into a seven-level one because of the splitting of the $J = 1$ levels. The $|3\rangle$ level splits into three components (Fig. 5), which results in the existence of three transitions to the $|1\rangle$ level allowed by the selection rules for radiative transitions. The probability of each of these transitions equals one-third of the total probability of the $|3\rangle \leftrightarrow |1\rangle$ transition. Similarly, the $|2\rangle$ level also splits into three components, and, according to the selection rules, the $|3\rangle \leftrightarrow |2\rangle$ transition transforms into six transitions, the probability of each of them being one-sixth of the total probability of the $|3\rangle \leftrightarrow |2\rangle$ transition.

An additional decay channel in multilevel systems compared with three-level ones is collisional depolarization [18]. The depolarization of an atom caused by a collision with another atom is related to transitions between states with different magnetic moment projections onto the selected direction. When a magnetic field is applied, collisions cause transitions between Zeeman sublevels with different magnetic momentum projections for each multiplet, $|m\rangle \rightleftharpoons |m \pm 1\rangle$. Collisions

Table 2. Samarium energy levels determining absorption spectrum

Even levels $4f^6 6s^2 ({}^7F)$				Odd level $4f^6 ({}^7F) 6s6p ({}^3P^0) {}^9F_1^0$		
J	Energy, cm ⁻¹	g	Relative population at $T = 600^\circ\text{C}$	J	Energy, cm ⁻¹	g
0	0	–	1.0			
1	292.58	1.50	0.6	1	14863.85	3.10
2	811.92	1.50	0.24			

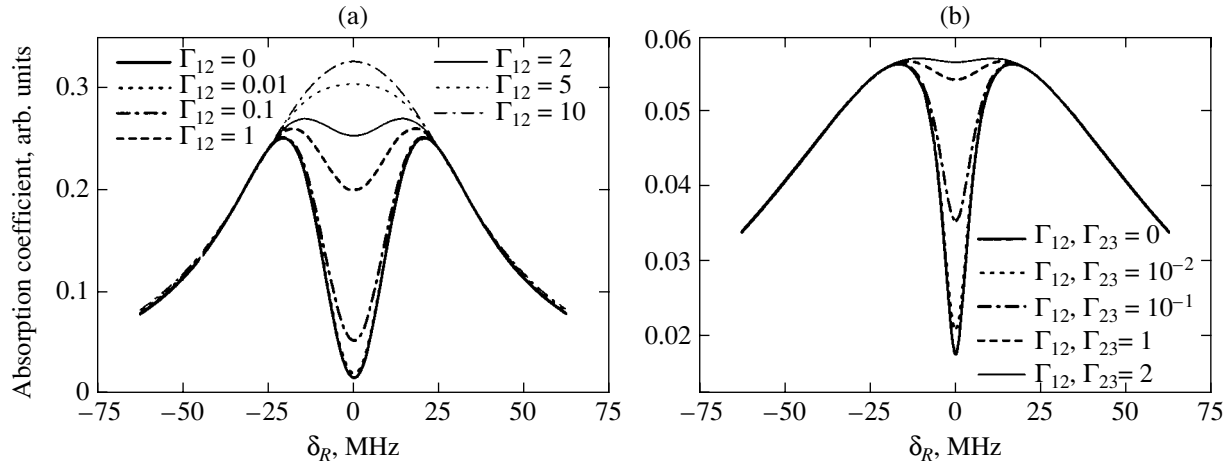


Fig. 4. Probing field absorption coefficients in (a) three-level and (b) four-level systems as functions of Raman detuning δ_R at $\delta_L = 0$ and different dephasing rates (s^{-1}). The corresponding schemes of levels are given in Figs. 1 and 2.

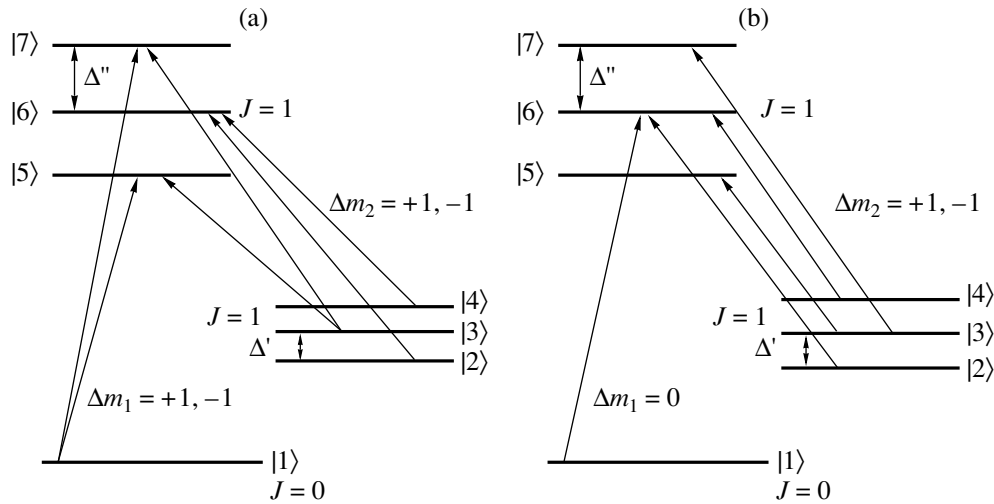


Fig. 5. Scheme of the Λ system of a samarium atom under applied (a) longitudinal magnetic field for linear orthogonal laser beam polarizations and (b) transverse magnetic field; the selection rules for the first field are $\omega_{L1} - \Delta m_1 = \pm 1$ (a) and 0 (b); for the second field, $\omega_{L2} - \Delta m_2 = \pm 1$; Δ' and Δ'' are the Zeeman splittings of the lower and upper levels with $J \neq 0$, respectively.

with changes in momentum projections destroy the coherence of the lower Λ system levels, which influences the coherent population trapping resonance value. We used the numerical data given in Section 6 to perform theoretical calculations. In the calculations, this process was taken into account by introducing depolarization constant G between the levels of each multiplet. This constant was used as an adjustable parameter and was varied in the range $G = 0-80\gamma_{41}$.

Below, we will distinguish between two applied magnetic field configurations, namely, longitudinal and transverse.

7.2. Longitudinal Magnetic Field

A scheme of levels for the longitudinal field configuration is shown in Fig. 5a. According to the selection

rules, six transitions are allowed for linearly polarized fields in the system under consideration, because $E_1 \perp H$ ($\Delta m_1 = \pm 1$) and $E_2 \perp H$ ($\Delta m_2 = \pm 1$). The $|1\rangle \leftrightarrow |5\rangle$, $|3\rangle \leftrightarrow |5\rangle$ and $|1\rangle \leftrightarrow |7\rangle$, $|3\rangle \leftrightarrow |7\rangle$ transitions form two Λ systems, whereas the $|2\rangle \leftrightarrow |6\rangle$ and $|4\rangle \leftrightarrow |6\rangle$ transitions, which are also allowed by the selection

Table 3. Parameters determining Λ system excitation

Rabi frequency, s^{-1}	Radiative decay rate, s^{-1}	Dephasing rate, s^{-1}
$\Omega_{14} = 0.58 \times 10^7$	$\gamma_{41} = 0.42 \times 10^6$	$\Gamma_{12} = 2.4 \times 10^4$
$\Omega_{24} = 0.83 \times 10^7$	$\gamma_{42} = 0.45 \times 10^6$	$\Gamma_{23} = 1.6 \times 10^4$
—	$\gamma_{43} = 0.42 \times 10^6$	—

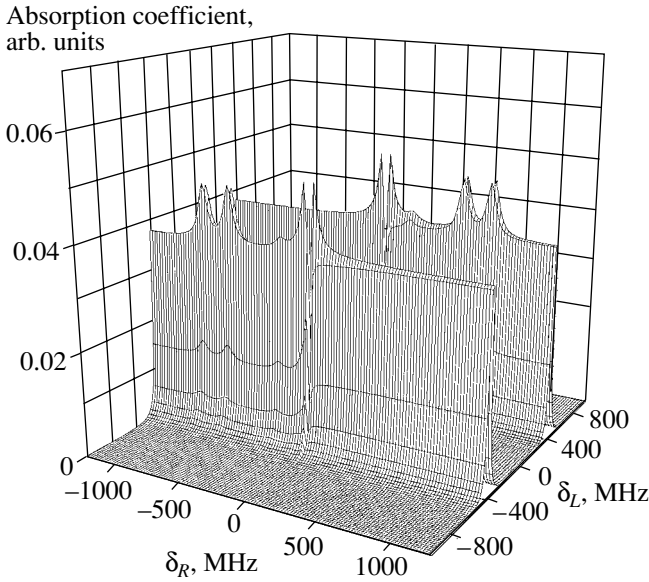


Fig. 6. Dependence of the absorption coefficient of the samarium atom at rest on δ_R and δ_L in applied longitudinal magnetic field.

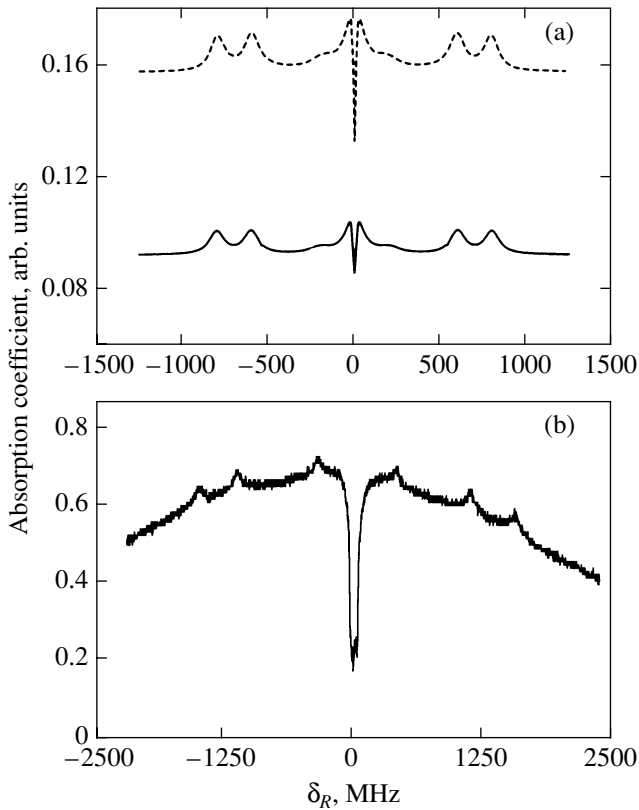


Fig. 7. (a) Theoretical dependences of the absorption coefficient of a seven-level system on Raman detuning δ_R in a longitudinal magnetic field calculated taking into account the Doppler effect at two temperatures $T = 10$ K (dashed line) and $T = 873$ K (solid line) and (b) experimental dependence of absorption coefficient in a 29 Oe longitudinal magnetic field at a 0.2 Torr buffer gas (Ar) pressure.

rules, do not participate in Λ system formation but are responsible for the formation of additional absorption peaks (see Appendix).

The dependence of the absorption coefficient of the samarium atom at rest on the Raman δ_R and laser δ_L detunings for the configuration under consideration is shown in Fig. 6; this dependence does not take into account depolarization. Including depolarization results, first, in an increase in induced absorption and, second, in a monotonic decrease in the contrast of coherent population trapping resonances. We observe hardly any depolarization effects on the width of coherent population trapping resonances.

We used (11) and the calculated absorption of the atom at rest to determine the absorption coefficient of the medium. The dependences of the absorption coefficient of the medium at $\omega_{L1} = \text{const}$ and $\delta_L = 0$ on the Raman detuning δ_R are shown in Fig. 7a for two temperatures, $T_1 = 873$ K (experimental temperature) and $T_2 = 10$ K.

Temperature variations change the absorption coefficient magnitude but have virtually no effect on its form. The reason for these changes is a temperature-induced increase in the contribution of atoms that interact with the field at large laser detunings, which decreases absorption $K(\delta_L, \delta_R)$.

For comparison, the experimental absorption spectrum of the probing laser field (672 nm, $\delta_L = 0$) obtained by scanning the frequency of the second controlling field is shown in Fig. 7b. According to Fig. 7, the typical width of experimentally observed coherent population trapping resonances is 5–6 MHz, which is in agreement with theoretical estimates. Because field absorption is measured at a fixed ω_{L1} frequency tuned in resonance with the atomic transition, the total width of the absorption contour as a function of the δ_R Raman detuning is unbounded.

The estimates given in the Appendix show that applying longitudinal magnetic field should split the coherent population trapping resonance by $2\Delta'\omega_{12}/\omega_{13}$. The positions of coherent population trapping resonances observed experimentally are in close agreement with these results, and the splitting amounts to about 3 MHz.

The experimentally observed broad absorption contour wings at large Raman detunings δ_R are explained by the influence of collisions [17], namely, by the possibility of the transfer of atoms from different speed groups to the group resonant to the light field [19]. This mechanism was not taken into account in our calculations.

7.3. Transverse Magnetic Field

The energy level diagram for the samarium atom in a transverse magnetic field is shown in Fig. 5b. Linearly polarized laser radiation with frequency ω_{L1} can only

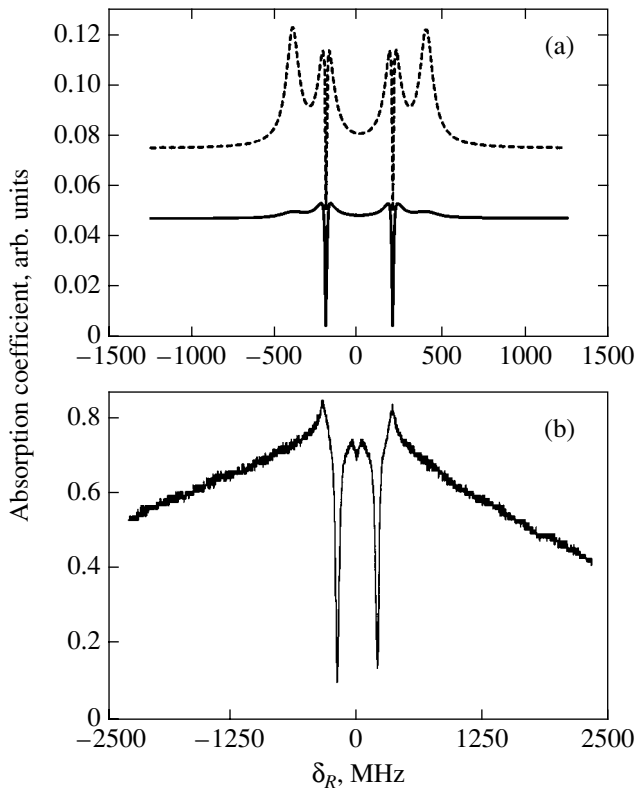


Fig. 8. (a) Theoretical dependences of the absorption coefficient of a seven-level system on Raman detuning δ_R in a transverse magnetic field calculated taking into account the Doppler effect at $T = 873$ K for two magnetic sublevel depolarization values, $G = 0$ (solid line) and $G = 0.5$ (dashed line) and (b) experimental dependence of the absorption coefficient in a 29 Oe transverse magnetic field at a 0.2 Torr buffer gas (Ar) pressure.

cause transitions with $\Delta m = 0$ (π components) in transverse magnetic field H_{\perp} (the H_{\perp} vector lies in the polarization plane). At the same time, laser radiation with frequency ω_{L2} and the polarization plane orthogonal to H_{\perp} causes transitions with $\Delta m = \pm 1$ (σ components). Two Λ systems (the transitions $|1\rangle \leftrightarrow |6\rangle$, $|2\rangle \leftrightarrow |6\rangle$ and $|1\rangle \leftrightarrow |6\rangle$, $|4\rangle \leftrightarrow |6\rangle$) are then formed. The $|3\rangle \leftrightarrow |5\rangle$ and $|3\rangle \leftrightarrow |7\rangle$ transitions do not participate in Λ system formation.

The absorption coefficients of the atom at rest, the depolarization effects, and the absorption coefficients of the medium taking into account the Doppler effect were calculated for the system in a transverse magnetic field using the approach described in Section 4.

The special feature of absorption spectra in a transverse magnetic field is the splitting of the coherent population trapping resonance line. The splitting of the resonance coincides with the Zeeman splitting value for level $J = 1$ sublevels $|2\rangle$ and $|4\rangle$, $\Delta\omega = 2\Delta'$ (see Appendix).

The depolarization of magnetic sublevels manifests itself similarly to the case of a longitudinal magnetic field (see Section 7.2). The resonance contrast is maxi-

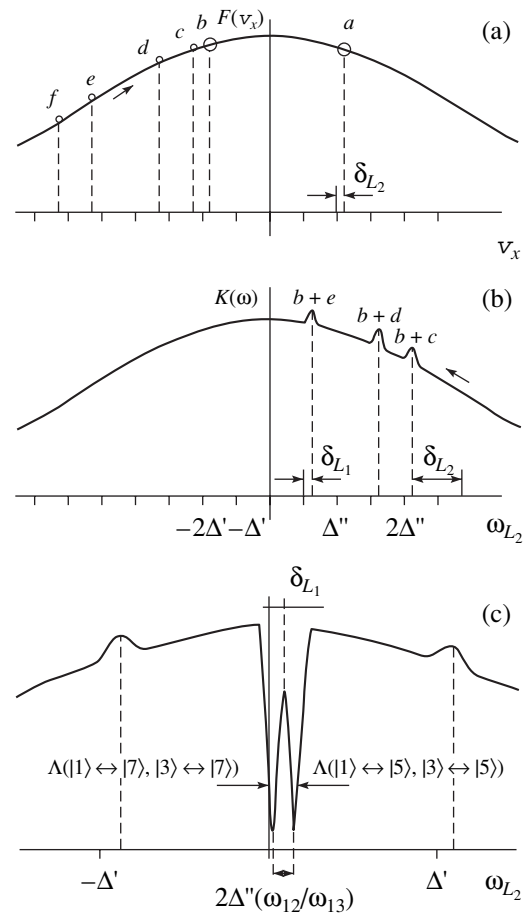


Fig. 9. Observation of coherent population trapping resonances against the background of a Doppler-broadened line; point a corresponds to the $|1\rangle \leftrightarrow |7\rangle$; b , to $|1\rangle \leftrightarrow |5\rangle$; c , to $|3\rangle \leftrightarrow |7\rangle$; d , to $|2\rangle \leftrightarrow |6\rangle$; e , to $|4\rangle \leftrightarrow |6\rangle$; and f , to the $|3\rangle \leftrightarrow |5\rangle$ transition. (a) $F(v_x)$ is the Maxwell velocity distribution function, points a and b correspond to particles with a definite velocity projection onto the beam propagation direction, namely, the projection at which the Doppler shift balances the detuning of field ω_{L1} frequency from the $|1\rangle \leftrightarrow |7\rangle$ and $|1\rangle \leftrightarrow |5\rangle$ quantum transition frequencies, respectively; points c , d , e , and f correspond to the velocity groups of particles for which the Doppler shift balances detuning δ_{L2} of frequency ω_{L2} from the $|3\rangle \leftrightarrow |7\rangle$, $|2\rangle \leftrightarrow |6\rangle$, $|4\rangle \leftrightarrow |6\rangle$, and $|3\rangle \leftrightarrow |5\rangle$ quantum transition frequencies, respectively; (b) illustration of the formation of absorption peaks $K(\omega)$; and (c) illustration of the formation of coherent population trapping resonances against the background of a Doppler-broadened line.

mum at $G = 0$; it decreases as G grows, but its width remains virtually constant.

The experimental data are compared with the theoretically calculated absorption coefficients of the medium in a transverse magnetic field in Fig. 8. As with a longitudinal magnetic field, the positions and widths of coherent population trapping resonances observed experimentally coincide with those found in theoretical calculations (see Appendix).

8. CONCLUSIONS

APPENDIX

In this work, we suggested a theoretical model for describing coherent population trapping in multilevel systems that allows calculations to be performed using a minimal set of input parameters. An analysis of the spectroscopic characteristics of coherent population trapping in samarium vapor in terms of this model showed that coherent population trapping resonances in the absence of an external magnetic field could well be approximated by a simple four-level model.

When a longitudinal or transverse magnetic field was applied, the spectroscopic characteristics of samarium atoms were well described by a seven-level model. The complication of the energy structure of samarium atom levels increased the number of coherent population trapping resonances and caused the appearance of additional peaks in the spectra, because the system under consideration decomposed into a set of three-level Λ systems, each being responsible for the formation of a resonance of its own. The transitions between the levels that did not directly participate in the formation of Λ systems contributed to the formation of induced absorption peaks.

In the presence of magnetic field, the depolarization of magnetic sublevels substantially influenced the shape of the absorption line and the contrast of coherent population trapping resonances, namely, the contrast of coherent population trapping resonances monotonically decreased as the depolarization constant increased.

The absorption coefficients of vapor were calculated taking into account the Maxwell velocity distribution of atoms and compared with the experimental data. It was shown that temperature variations caused changes in the absorption coefficient magnitude but had almost no effect on its form.

The results of numerical calculations accurately reproduced the experimental data on coherent population trapping resonance positions and widths and on the shape of the spectra obtained in the presence of a transverse magnetic field. Qualitatively, the theoretical estimates were also in agreement with the splitting of the coherent population trapping resonance by a small value of the order of 3 MHz observed experimentally in a longitudinal magnetic field. The reproduction of such a splitting in numerical calculations would, however, require going beyond the approximations [15] usually applied to describe the Doppler broadening effect on the formation of coherent population trapping spectra.

ACKNOWLEDGMENTS

This work was financially supported by the Russian Foundation for Basic Research (projects nos. 01-02-16311, 01-02-174-42, 01-02-174-39, 00-15-96-586), State Scientific-Technical Program "Fundamental Metrology," INTAS (INFO 00-479), and Volkswagen-Stiftung (I/73647).

FEATURES OF COHERENT POPULATION TRAPPING RESONANCES AGAINST THE BACKGROUND OF A DOPPLER-BROADENED LINE IN MAGNETIC FIELDS

Longitudinal Magnetic Field

In experiments, the frequency of the first laser is constant and equal to $\omega_{L1} = \omega_{13} + \delta_{L1}$, where δ_{L1} is a small laser detuning. Only the particles that have a certain velocity projection along the light beam direction can be in resonance with field ω_{L1} . This projection is determined by the condition that the Doppler shift should balance the detuning of field ω_{L1} from the frequencies of the $|1\rangle \longleftrightarrow |7\rangle$ and $|1\rangle \longleftrightarrow |5\rangle$ quantum transitions (points *a* and *b* in Fig. 9a).

The absorption of wave ω_{L1} is observed at the frequencies $\omega_{13} + \Delta''$ (the $|1\rangle \longleftrightarrow |7\rangle$ transition) and $\omega_{13} - \Delta''$ (the $|1\rangle \longleftrightarrow |5\rangle$ transition). According to the definition of the Doppler effect, the corresponding group velocities are

$$\omega_{L1} = \frac{\omega_{13} + \Delta''}{1 - v_{x1}/c}$$

$$\rightarrow \left(1 - \frac{v_{x1}}{c}\right) = \frac{\omega_{13} + \Delta''}{\omega_{L1}} \quad (\text{point } a),$$

$$\omega_{L1} = \frac{\omega_{13} - \Delta''}{1 - v_{x2}/c}$$

$$\rightarrow \left(1 - \frac{v_{x2}}{c}\right) = \frac{\omega_{13} - \Delta''}{\omega_{L1}} \quad (\text{point } b).$$

The interaction of particles in each velocity group with field ω_{L1} depletes level $|1\rangle$, whereas the populations of levels $|2\rangle$, $|3\rangle$, and $|4\rangle$ increase because of upper level decays. The second frequency $\omega_{L2} = \omega_{23} + \delta_{L2}$, where δ_{L2} is the detuning of the second field, is scanned in a wide frequency range. The *c*, *d*, *e*, and *f* points in Fig. 9a correspond to the velocity groups of particles for which the Doppler shift balances the δ_{L2} detuning of frequency ω_{L2} from the $|3\rangle \longleftrightarrow |7\rangle$, $|2\rangle \longleftrightarrow |6\rangle$, $|4\rangle \longleftrightarrow |6\rangle$, and $|3\rangle \longleftrightarrow |5\rangle$ quantum transition frequencies. The absorption of wave ω_{L2} is observed at four frequencies, namely, $\omega_{23} \pm \Delta''$ (the $|3\rangle \longleftrightarrow |7\rangle$ and $|3\rangle \longleftrightarrow |5\rangle$ transitions) and $\omega_{23} \pm \Delta'$ ($|2\rangle \longleftrightarrow |6\rangle$ and $|4\rangle \longleftrightarrow |6\rangle$ transitions); that is, the equations for the corresponding velocity groups have the form

$$\omega_{L2} = \frac{\omega_{23} + \Delta''}{1 - v_{x3}/c}$$

$$\rightarrow \left(1 - \frac{v_{x3}}{c}\right) = \frac{\omega_{23} + \Delta''}{\omega_{L2}} \quad (\text{point } c),$$

$$\begin{aligned} \omega_{L2} &= \frac{\omega_{23} + \Delta'}{1 - v_{x4}/c} \\ \longrightarrow \left(1 - \frac{v_{x4}}{c}\right) &= \frac{\omega_{23} + \Delta'}{\omega_{L2}} \quad (\text{point } d), \\ \omega_{L2} &= \frac{\omega_{23} - \Delta'}{1 - v_{x5}/c} \\ \longrightarrow \left(1 - \frac{v_{x5}}{c}\right) &= \frac{\omega_{23} - \Delta'}{\omega_{L2}} \quad (\text{point } e), \\ \omega_{L2} &= \frac{\omega_{23} - \Delta''}{1 - v_{x6}/c} \\ \longrightarrow \left(1 - \frac{v_{x6}}{c}\right) &= \frac{\omega_{23} - \Delta''}{\omega_{L2}} \quad (\text{point } f). \end{aligned}$$

If the detuning δ_{L_2} is larger than $\omega_{23} + \Delta''$, points c – f are situated to the left of point b . In all these velocity groups (a – f), atoms are excited by radiation ω_{L2} or ω_{L1} . Equilibrium population distribution is disturbed. The c , d , e , and f plot points (Fig. 9a) move to the right as detuning δ_{L_2} decreases. When points c and b coincide, the atoms in these velocity groups simultaneously interact with both fields. Two transitions that do not form a Λ system are excited, but, because the distribution of particles over levels is nonequilibrium and level $|3\rangle$ is populated excessively, the absorption of the second wave increases, which corresponds to an absorption peak (Fig. 9b). The frequency of this absorption peak can be determined from the condition of the coincidence of velocity groups v_{x2} (point b) and v_{x3} (point c); that is, from the condition

$$\frac{\omega_{13} - \Delta''}{\omega_{L1}} = \frac{\omega_{23} + \Delta''}{\omega_{L2}}.$$

Using this equation, we easily find the frequency at which the first absorption peak is observed, $\omega_{L2} = \omega_{23} + 2\Delta'' + \delta_{L_1}$. Decreasing δ_{L_2} further, we observe absorption peaks corresponding to the coincidence of the v_{x2} and v_{x4} (points b and d) and v_{x2} and v_{x5} (points b and e) velocity groups. The corresponding frequencies are $\omega_{L2} = \omega_{23} + \Delta'' + \Delta' + \delta_{L_1}$ and $\omega_{L2} = \omega_{23} + \Delta' + \delta_{L_1}$. Decreasing δ_{L_2} further brings points c and a in coincidence, which corresponds to simultaneous excitation of the $|1\rangle \longleftrightarrow |7\rangle$ and $|3\rangle \longleftrightarrow |7\rangle$ transitions, that is, to a coherent population trapping resonance in the Λ system formed by the $|1\rangle$, $|3\rangle$, and $|7\rangle$ levels. Let us calculate the frequency of the coherent population trapping resonance peak. The condition of the coincidence of velocity groups v_{x1} and v_{x3} is

$$\left(1 - \frac{v_{x1}}{c}\right) = \frac{\omega_{13} + \Delta''}{\omega_{L1}}, \quad \left(1 - \frac{v_{x3}}{c}\right) = \frac{\omega_{23} + \Delta''}{\omega_{L2}}.$$

It follows that the first coherent population trapping resonance is observed at the frequency

$$\omega_{L2} = \omega_{23} + \delta_{L_1} + \frac{\omega_{12}\Delta''}{\omega_{13}}.$$

The second coherent population trapping resonance arises when the v_{x6} (point f) and v_{x2} (point b) velocity groups coincide. Accordingly, we obtain the frequency of the second coherent population trapping resonance peak in the form

$$\omega_{L2} = \omega_{23} + \delta_{L_1} - \frac{\omega_{12}\Delta''}{\omega_{13}}.$$

The distance between the two coherent population trapping resonances is

$$\omega_{L2}^{ac} - \omega_{L2}^{bf} = 2\Delta' \frac{\omega_{12}}{\omega_{13}}.$$

A further decrease in δ_{L_2} results in the appearance of absorption peaks in the left part of the plot (Fig. 9c). Note that the laser detuning of the second field being nonzero results in that the distribution of peaks and resonances is symmetrical with respect to the frequency

$$\omega_{L2} = \omega_{23} + \delta_{L_1}. \quad (\text{A.1})$$

To summarize, we observe six absorption peaks and two coherent population trapping resonances symmetrically distributed with respect to the (A.1) frequency on a Doppler broadened contour, which differs from the picture characteristic of an atom at rest.

Transverse Magnetic Field

The reasoning is similar to that with a longitudinal magnetic field. The absorption of wave ω_{L1} is observed at the ω_{13} frequency (the $|1\rangle \longleftrightarrow |6\rangle$ transition). The second frequency $\omega_{L2} = \omega_{23} + \delta_{L_2}$, where δ_{L_2} is the detuning of the second field, is scanned in a wide frequency range. The absorption of wave ω_{L2} is observed at two frequencies, namely, $\omega_{23} \pm \Delta'$ (the $|2\rangle \longleftrightarrow |6\rangle$ and $|4\rangle \longleftrightarrow |6\rangle$ transitions). Simultaneous excitation of the $|1\rangle \longleftrightarrow |6\rangle$ and $|2\rangle \longleftrightarrow |6\rangle$ transitions and of the $|1\rangle \longleftrightarrow |6\rangle$ and $|4\rangle \longleftrightarrow |6\rangle$ transitions corresponds to coherent population trapping resonances in the Λ systems formed by the $|1\rangle$, $|6\rangle$, $|2\rangle$ and $|1\rangle$, $|6\rangle$, $|4\rangle$ levels, respectively. It follows that two coherent population trapping resonances are observed at the $\omega_{L2} = \omega_{23} \pm \Delta'$ frequencies. The distance between the resonances equals twice the Zeeman splitting of the lower level, that is, $\Delta\omega_{\perp} = 2\Delta'$. Note that the ratio between the splittings of coherent population trapping resonances for

samarium in transverse and longitudinal magnetic fields is

$$\frac{\Delta\omega_{\perp}}{\Delta\omega_{\parallel}} = \frac{2\Delta'_{\perp}}{2\Delta'_{\parallel}\omega_{12}/\omega_{13}} = 25\frac{H_{\perp}}{H_{\parallel}}.$$

REFERENCES

1. E. Arimondo, in *Progress in Optics*, Ed. by E. Wolf (Elsevier, Amsterdam, 1996), Vol. 35, p. 257.
2. G. Alzetta, A. Gozzini, L. Moi, and G. Orriols, *Nuovo Cimento B* **36**, 5 (1976).
3. H. R. Gray, R. M. Whitly, and C. R. Stroud, Jr., *Opt. Lett.* **3**, 218 (1978).
4. G. Alzetta, L. Moi, and G. Orriols, *Nuovo Cimento B* **52**, 209 (1979); *Opt. Commun.* **42**, 335 (1982).
5. A. Aspect, E. Arimondo, R. Kaiser, *et al.*, *Phys. Rev. Lett.* **61**, 826 (1988).
6. A. Kasapi, *Phys. Rev. Lett.* **77**, 1035 (1996).
7. R. Wynands and A. Nagel, *Appl. Phys. B* **68**, 1 (1999).
8. R. Holtzwarth, Th. Udem, and T. W. Haensch, *Phys. Rev. Lett.* **85**, 2264 (2000).
9. N. N. Kolachevskii, A. V. Akimov, N. A. Kiselev, *et al.*, *Kvantovaya Élektron. (Moscow)* **31** (1), 61 (2001).
10. B. A. Grishanin, <http://comsim1.phys.msu.ru/people/grishanin/teaching/qsp/>.
11. L. A. Vainshtein, I. I. Sobel'man, and E. A. Yukov, *Excitation of Atoms and Broadening of Spectral Lines* (Nauka, Moscow, 1978; Springer, Berlin, 1981).
12. W. Happer, *Rev. Mod. Phys.* **44**, 169 (1972).
13. B. A. Grishanin, V. N. Zadkov, and D. Meschede, *Phys. Rev. A* **58**, 4235 (1998).
14. I. V. Bargatin, B. A. Grishanin, and V. N. Zadkov, *Proc. SPIE* **3736**, 246 (1998).
15. E. Kuznetsova, O. Kocharovskaya, and M. O. Scully, *Proc. SPIE* **4750**, 117 (2002).
16. N. N. Kolachevskii, A. V. Akimov, N. A. Kiselev, *et al.*, *Opt. Spektrosk.* **90** (2), 201 (2001) [*Opt. Spectrosc.* **90**, 164 (2001)].
17. A. V. Akimov, N. N. Kolachevsky, V. N. Sorokin, and S. I. Kanorsky, in *Abstracts of International Quantum Electronics Conference, IQEC-2002, Technical Digest* (Moscow, 2002), p. 93.
18. B. M. Smirnov, *Excited Atoms* (Énergoizdat, Moscow, 1982).
19. P. F. Liao, J. E. Bjorkholm, and P. R. Berman, *Phys. Rev. A* **21** (6), 1927 (1980).

Translated by V. Sipachev